Effect of La and Tb Substitution on the Structure, Hydration, and Electrical Properties of NBSCF Triple-Conducting Perovskite Oxides

Ghaida Al Sulami | Supervised by: Dr. Peng Ren, Prof. Yoji Kobayashi
King Abdullah University of Science and Technology (KAUST), KCC Division, Saudi Arabia

Table of Contents

1. Introduction 2
2. Related Work 2
3. Methodology 2
    3.1 Method Details 2
    3.2 Evaluation Procedure 3
4. Results 3
    4.1 Composition Library 3
    4.2 Structural Results — Nd End-Member (Synchrotron XRD + PDF) 4
    4.3 Laboratory XRD — Nd–La and Nd–Tb Series 8
    4.4 Hydration Behavior (TGA) — Nd End-Member 10
    4.5 HRTEM and FFT — Nd End-Member 11
    4.6 DC Conductivity 12
5. Discussion 13
6. Limitations and Future Work 13
7. Conclusion 14
References 14

1. Introduction

Hydrogen is a key vector for decarbonizing hard-to-electrify sectors, but its production cost and efficiency depend strongly on the electrochemical devices used to make it. Solid oxide electrolysis cells (SOECs) split water into hydrogen and oxygen using an oxide-ion-conducting electrolyte, typically at 700–900 °C. Protonic ceramic electrolysis cells (PCECs) instead use a proton-conducting electrolyte and can operate at 400–600 °C — a substantially milder temperature range that reduces thermal degradation and balance-of-plant cost, provided the electrode materials can sustain competitive current densities at lower temperature.

The performance of PCECs is generally limited by the air electrode, where oxygen reduction/evolution kinetics are sluggish. Triple-conducting oxides — materials that simultaneously transport electrons/holes, oxide ions, and protons — can extend the electrochemically active zone across the entire electrode surface rather than confining it to the electrode/electrolyte/gas triple-phase boundary, and are therefore attractive air-electrode candidates for PCECs.

This project investigates a family of Ba/Sr/Co/Fe-based triple-conducting perovskite oxides with the fixed framework Ba0.5Sr0.5Co1.5Fe0.5O5+δ (BSCF), in which the lanthanide (Ln) A-site cation is systematically varied. The scientific motivation is that the Ln3+ ionic radius should influence the average crystal structure, cation ordering, oxygen coordination, and oxygen-vacancy concentration — and, through these, the oxide-ion and proton transport pathways relevant to PCEC and protonic ceramic fuel cell (PCFC) operation. Four Ln-substitution families were targeted: PrxTb1-x, NdxTb1-x, NdxLa1-x, and PrxLa1-x (BaSCF), each at x = 0, 0.25, 0.50, 0.75, giving 16 nominal compositions.

This report documents the work completed to date: (i) synthesis of the full 16-composition library, (ii) synchrotron XRD and PDF structural characterization of the Nd end-member (NBSCF), (iii) laboratory XRD across eight further compositions spanning the Nd–La and Nd–Tb series, (iv) thermogravimetric hydration behavior, (v) HRTEM lattice imaging, and (vi) room-temperature DC conductivity for four compositions. Results are reported exactly as measured; where full structural refinement or electrochemical testing has not yet been performed, this is stated explicitly rather than estimated.

2. Related Work

Triple-conducting Ba/Sr/Co/Fe perovskites and related double perovskites have been studied extensively as air electrodes for protonic ceramic devices. Ding et al. demonstrated a self-sustainable, high-performance PCEC using a triple-conducting oxide air electrode, establishing the practical relevance of the electrode chemistry studied here [1]. Papac et al. reviewed the design principles and characterization strategies for triple-conducting oxides, highlighting how oxygen non-stoichiometry and A-site chemistry govern the balance between electronic, oxide-ion, and proton conduction [2]. Feldhoff et al. examined the related Ba0.5Sr0.5Co0.8Fe0.2O3-δ (BSCF) system for oxygen permeation membranes, providing a structural and defect-chemistry baseline for the Co/Fe-rich perovskite framework used here [3].

The ordered double-perovskite NdBaCo2O5+δ (space group P4/mmm), in which the Ln and alkaline-earth cations occupy separate A-site layers along the c-axis, is a well-documented structural motif for related Ln-Ba-Co-O materials and provided the reference framework this project's real-space structural comparisons were built against.

Research gap: while individual end-member compositions in this family have been reported, a systematic map of how the Ln-site ionic radius (from the larger La3+ down to the smaller Tb3+) shifts the average and local structure, cation ordering, and oxygen-vacancy content — within one fixed Ba0.5Sr0.5Co1.5Fe0.5O5+δ framework — has not been established. This project addresses that gap.

3. Methodology

3.1 Method Details

Powder synthesis. All 16 nominal compositions were synthesized by an EDTA–citrate complexing method. Stoichiometric metal nitrate precursors — Pr(NO3)3·6H2O, Nd(NO3)3·6H2O, La(NO3)3·6H2O, Tb(NO3)3·5H2O, Ba(NO3)2, Sr(NO3)2, Co(NO3)2·6H2O, and Fe(NO3)3·9H2O — were dissolved in deionized water. EDTA (C10H16N2O8) was dissolved separately in aqueous ammonia and combined with the metal-nitrate solution, after which citric acid monohydrate (C6H8O7·H2O) was added. The molar ratio of total metal ions : EDTA : citric acid was 4 : 1.2 : 2 (EDTA and citric acid each supplied in excess relative to the metal-ion total, consistent with the 4.8 and 6 mol equivalents used in the precursor calculations). Ammonia was used to adjust the solution to approximately pH 6. The solution was stirred and heated at ~120 °C for ~3 h to remove excess water and promote gel formation, after which the gel was thermally treated to remove organics and

calcined to form the target perovskite phase. Exact calcination temperature/time are not included in the experimental records available for this report and are not stated here.

Batch-size adjustments. Some compositions (notably three members of the PrxLa1-x series) were prepared at half the standard batch scale because of limited precursor powder availability, and one composition was scaled up threefold. These are documented as practical batch-size adjustments and do not correspond to any change in target stoichiometry.

Pellet fabrication. Powders were pressed into pellets using a Carver manual benchtop pellet press, using either a 6 mm-diameter die (~0.085 g powder) or a 10 mm-diameter die (~0.35 g powder). A sacrificial powder bed of matching composition was used during sintering where applicable to limit volatile-component loss.

3.2 Evaluation Procedure

Synchrotron XRD + PDF (Nd end-member only). High-energy synchrotron X-ray total scattering data were collected at ESRF ($\lambda = 0.1652$ Å) on the Nd end-member (NBSCF). Two independent Rietveld refinements were carried out in GSAS-II: (i) using the XRD histogram alone, and (ii) a joint refinement using the XRD and PDF histograms together. A separate, independent real-space fit of the PDF G(r) over the 1.5–20 Å range was carried out in PDFfit2 to probe the local structure. These three analyses are reported separately in Section 4 and are not combined.

Laboratory XRD (Nd–La and Nd–Tb series). Eight further compositions — NdxLa1-xBSCF at x = 0.25, 0.50, 0.75, 1.00 and NdxTb1-xBSCF at x = 0.25, 0.50, 0.75, 1.00 — were measured by laboratory powder XRD (Cu Kα, $\lambda = 1.5406$ Å, confirmed from the instrument export header). Full Rietveld refinement was not performed on this data set. Instead, a single-peak pseudo-cubic lattice parameter was estimated from the strongest reflection ($2\theta \approx 32–34°$, indexed as the pseudo-cubic (110)) via Bragg's law, $d = \lambda/(2 \sin \theta)$, and $a = d\sqrt{2}$. This approach assumes cubic symmetry and is explicitly an approximation, not a refinement; it is invalid for compositions where the reflection is resolved into multiple components (see Section 4.3).

Thermogravimetric analysis (Nd end-member only). TGA was performed on a NETZSCH STA 449 F1 instrument (26.7 mg NBSCF powder) from 30 to 800 °C under humid Ar, with isothermal holds at 300, 400, 500, 600, 700, and 800 °C. Mass change and residual mass were extracted directly from the raw exported data at each hold.

HRTEM (Nd end-member only). High-resolution TEM images were acquired on the NBSCF sample (files nbscf_1200_48H_0001 and _0002, pixel-calibrated at 0.0441 and 0.0176 nm/pixel respectively). Fast Fourier transforms (FFTs) were computed from a clean, defect-free 512 × 512-pixel region of image _0002; spot positions were converted to real-space d-spacings using the calibrated pixel size and compared against the (100) and (110) spacings expected from the refined cubic cell.

DC conductivity (four compositions). Two-terminal DC resistance was measured at room temperature for LaBSCF, NBSCF, Nd0.5Tb0.5BSCF, and TbBSCF pellets. Conductivity was calculated as $\sigma = H / (R \times A)$, where R is the measured resistance, H the pellet thickness, and A the electrode contact area.

4. Results

4.1 Composition Library

All 16 nominal compositions across the four Ln-substitution families were synthesized as powders and, where noted below, pressed into pellets. This composition library — together with the precursor calculations, batch-size adjustments, and pellet fabrication — constitutes the main completed synthesis contribution of this project.

Family	x = 0	x = 0.25	x = 0.50	x = 0.75
PrxTb1-x BSCF	TbBSCF	0.25Pr-0.75Tb	0.50Pr-0.50Tb	0.75Pr-0.25Tb
NdxTb1-x BSCF	TbBSCF	0.25Nd-0.75Tb	0.50Nd-0.50Tb	0.75Nd-0.25Tb
NdxLa1-x BSCF	LaBSCF	0.25Nd-0.75La	0.50Nd-0.50La	0.75Nd-0.25La
PrxLa1-x BSCF	LaBSCF	0.25Pr-0.75La	0.50Pr-0.50La	0.75Pr-0.25La

Characterization status: the Nd end-member (NBSCF) has full synchrotron XRD+PDF, TGA, and HRTEM data; eight further compositions (the NdxLa1-x and NdxTb1-x series) have laboratory XRD; four compositions (LaBSCF, NBSCF, Nd0.5Tb0.5BSCF, TbBSCF) have room-temperature DC conductivity. The PrxTb1-x and PrxLa1-x families currently have no characterization data beyond synthesis.

4.2 Structural Results — Nd End-Member (Synchrotron XRD + PDF)

Three independent analyses of the same NBSCF sample are reported separately below, as they are not equivalent and should not be averaged or combined.

Refinement	a (Å)	wR	GOF	O content (per f.u.)
XRD-only Rietveld	3.84904(2)	7.85%	11.3	2.85 / 3
Joint XRD + PDF Rietveld	3.84900	5.88%	8.47	2.57 / 3
Local PDF fit (1.5–20 Å)	3.8473(11)	8.94% (Rw)	0.0143 (red. χ2)	2.57 / 3

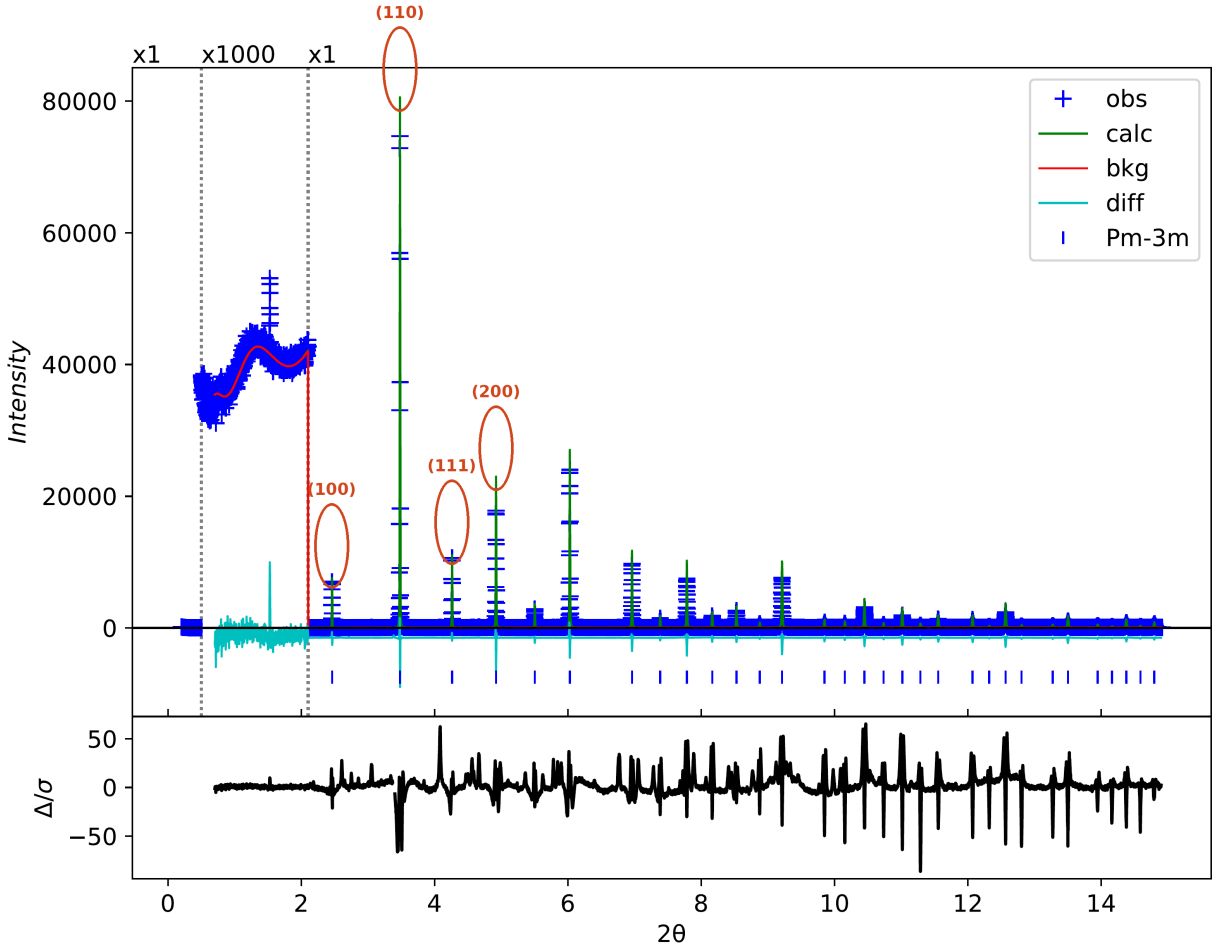


Figure 1. Rietveld fit (XRD-only) of NBSCF, cubic Pm-3m. Circled reflections are calculated from the refined cell via Bragg's law: (100) 2.459°, (110) 3.478°, (111) 4.260°, (200) 4.920° (λ = 0.1652 Å).

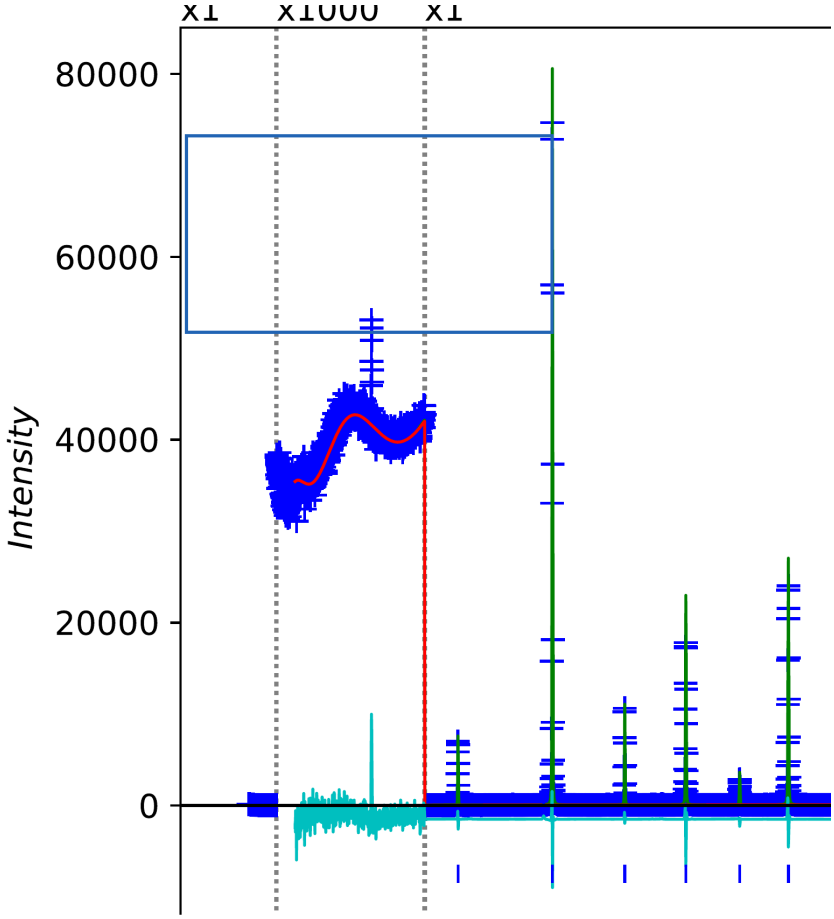


Figure 2. Low-angle region (×1000 magnification). No discrete superstructure/cation-ordering peak is observed above background, indicating no long-range A-site or B-site ordering is detected by XRD at the current resolution.

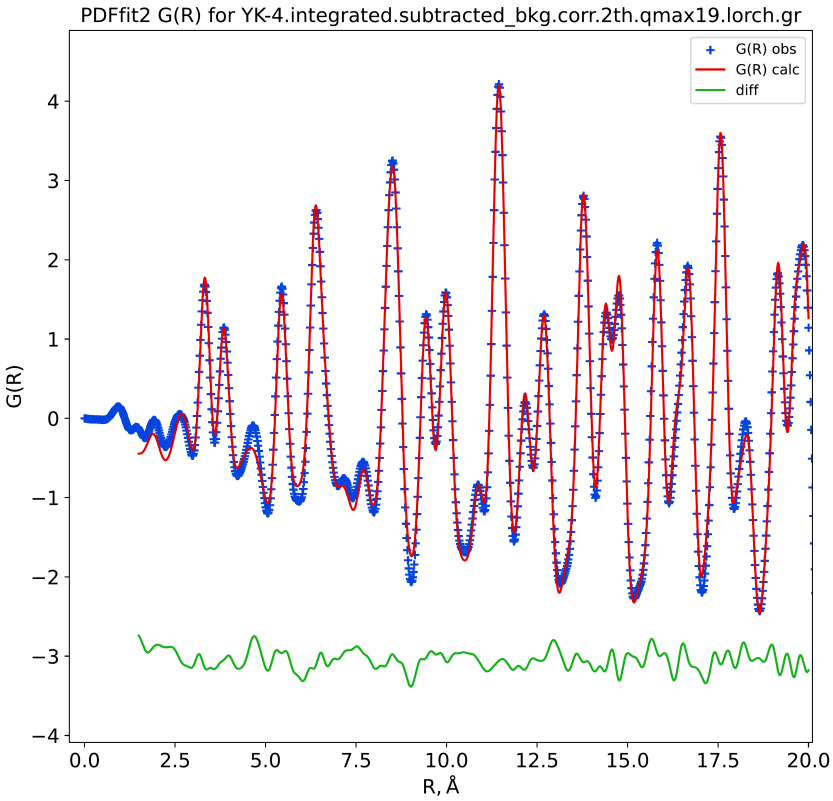


Figure 3. PDFfit2 real-space fit of G(r), 0–20 Å, cubic Pm-3m model. The local (PDF) and average (Rietveld) lattice parameters agree within ~0.05%.

Two structural models were compared directly from refined/candidate CIF files: the disordered cubic Pm-3m model (matching the joint XRD+PDF refinement, with Ba/Sr/Nd sharing one A-site and 86% oxygen occupancy on the anion site) and an A-site-ordered tetragonal P4/mmm model (a preliminary — "rough" — refinement in which Nd fully occupies one layer and Ba/Sr the other, analogous to the NdBaCo2O5+δ double-perovskite motif). Both are shown in Figure 4 for comparison; the tetragonal model is not yet a finalized refinement.

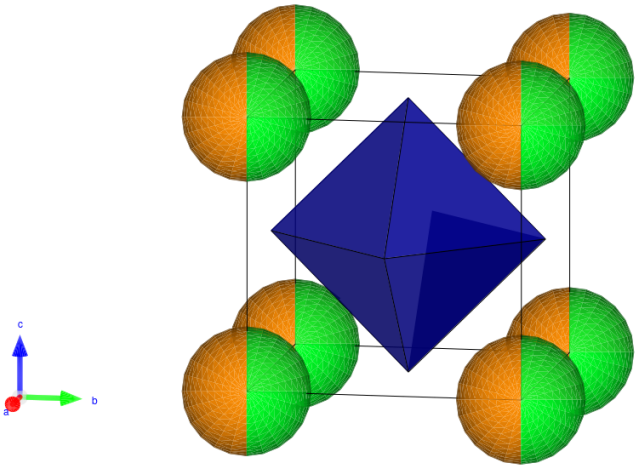


Figure 4a. Cubic Pm-3m NBSCF (disordered A-site), rendered from the refined CIF. Mixed occupancy shown as split-color spheres.

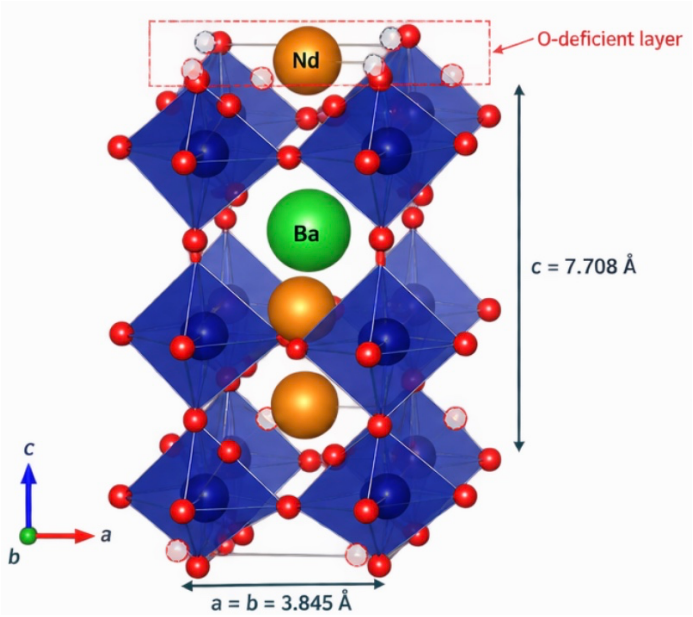


Figure 4b. Alternative A-site-ordered tetragonal P4/mmm model (preliminary refinement), same NBSCF composition.

4.3 Laboratory XRD — Nd–La and Nd–Tb Series

Stacked, normalized XRD patterns for the four NdxLa1-x and four NdxTb1-x compositions are shown in Figures 5 and 6. Both series show the expected perovskite reflection pattern; the Tb-rich compositions (75% and 100% Tb) show clear splitting of the main reflection into multiple resolved components (confirmed by peak-finding: e.g. TbBSCF shows components at 2θ = 32.93°, 33.28°, and 33.38° rather than a single peak), consistent with a lowering of symmetry away from cubic at high Tb content — in agreement with the alternative tetragonal structural model in Section 4.2.

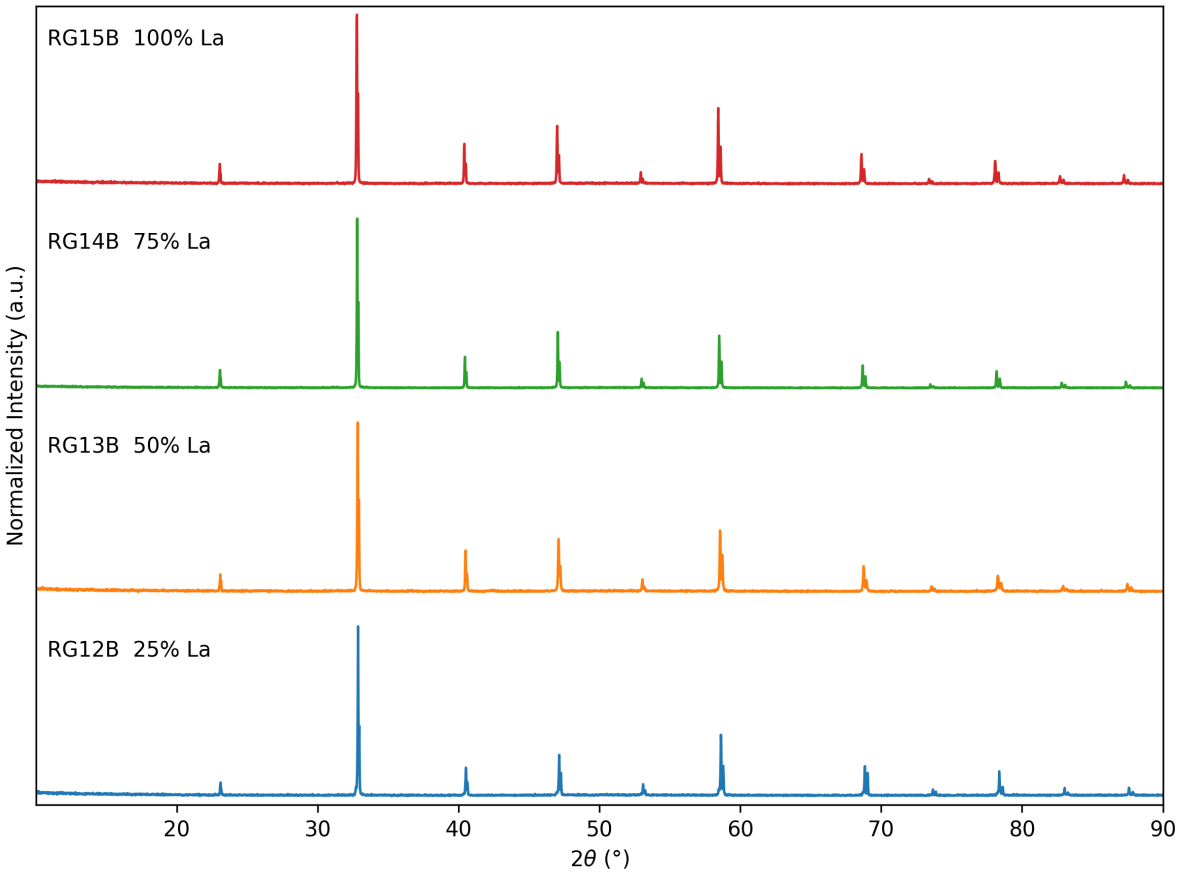


Figure 5. Stacked, normalized lab XRD (Cu Kα) for the NdxLa1-x series.

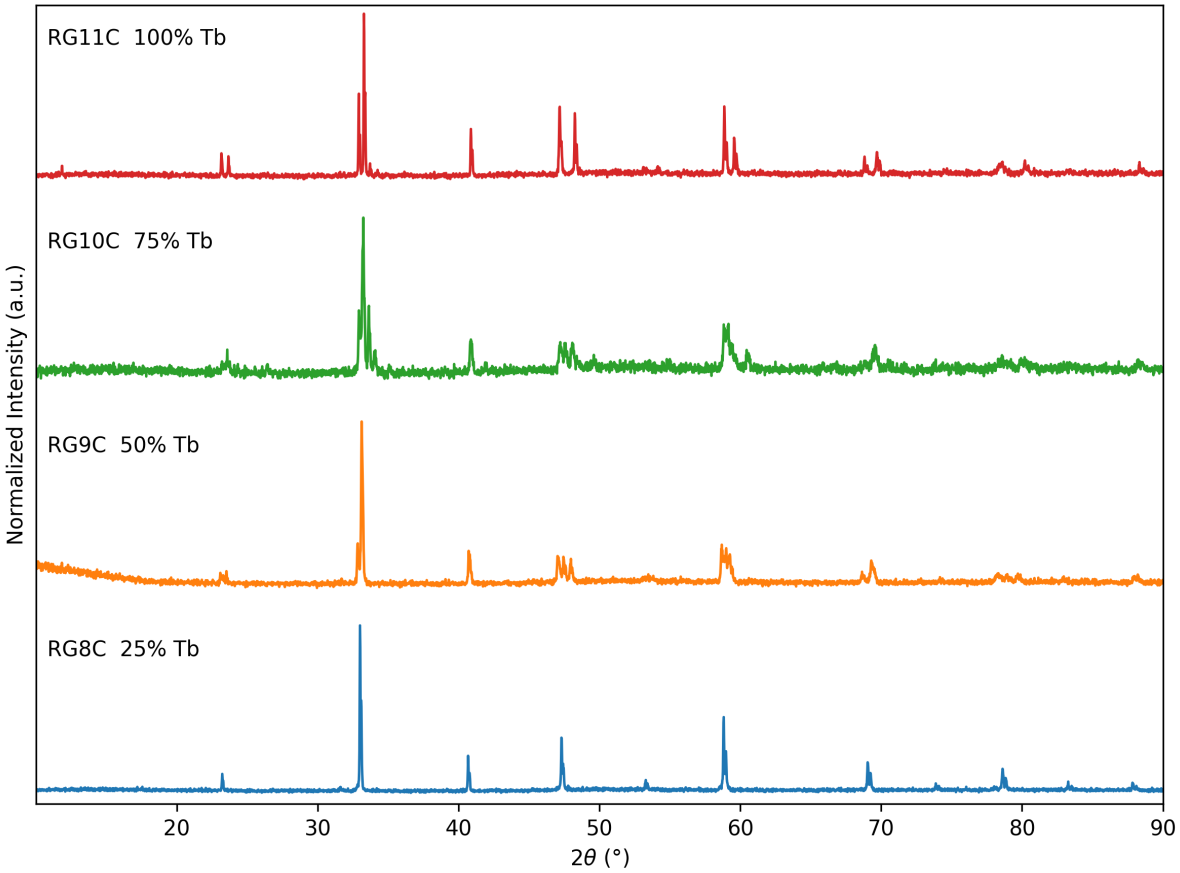


Figure 6. Stacked, normalized lab XRD (Cu Kα) for the NdxTb1-x series. Note the resolved peak splitting at 75% and 100% Tb.

Single-peak pseudo-cubic lattice parameters, extracted as described in Section 3.2, are given below and plotted in Figure 7 alongside the synchrotron-refined Nd end-member value for reference.

Sample	x (Ln fraction)	2θ main peak (°)	a, pseudo-cubic (Å)
Nd0.75La0.25BSCF	0.25 La	32.870	3.8503
Nd0.50La0.50BSCF	0.50 La	32.850	3.8527
Nd0.25La0.75BSCF	0.75 La	32.809	3.8573
LaBSCF	1.00 La	32.788	3.8597
Nd0.75Tb0.25BSCF	0.25 Tb	33.005	3.8351
Nd0.50Tb0.50BSCF	0.50 Tb	33.124	3.8217
Nd0.25Tb0.75BSCF*	0.75 Tb	33.243	3.8084
TbBSCF*	1.00 Tb	33.282	3.8040

**Peak splitting observed — single-peak value is an approximation (see Fig. 6).*

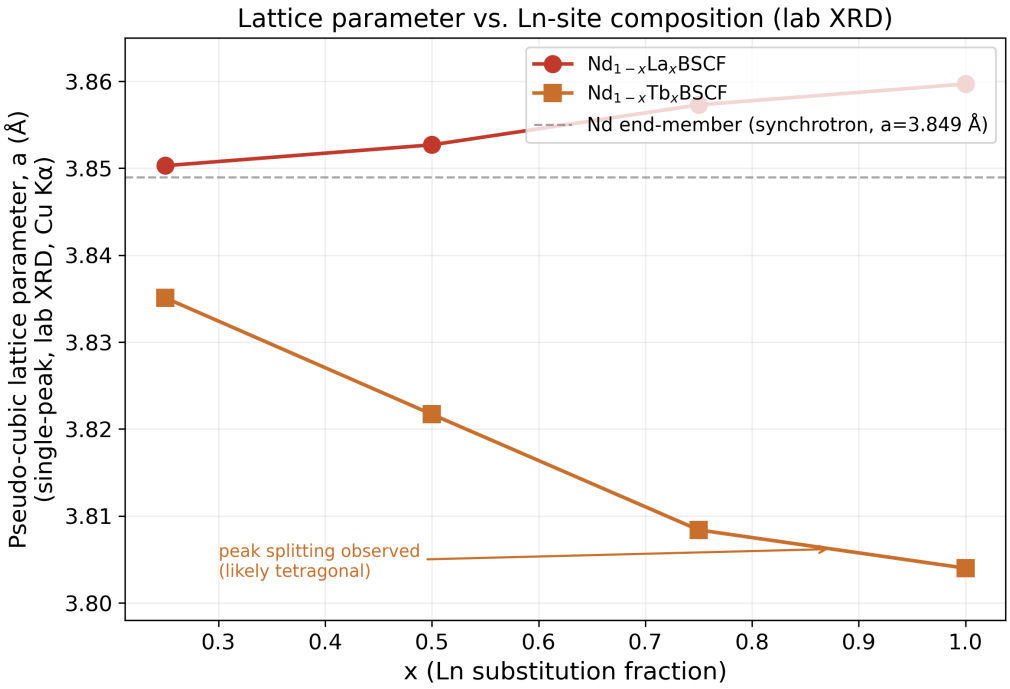


Figure 7. Pseudo-cubic lattice parameter vs. Ln substitution fraction for both series, referenced against the synchrotron-refined Nd end-member (dashed line). Lattice parameter increases with La substitution and decreases with Tb substitution, tracking Shannon ionic radii (La3+ > Nd3+ > Tb3+).

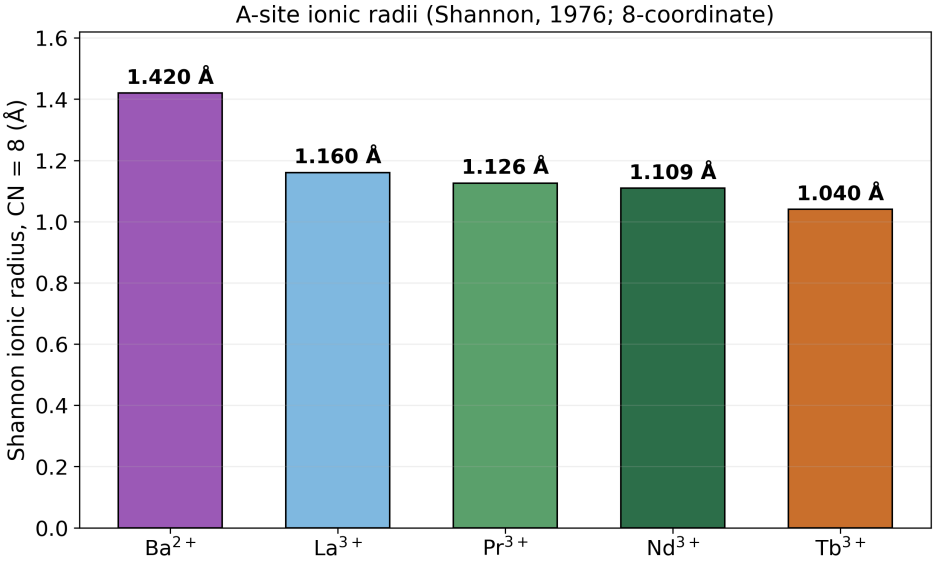


Figure 8. A-site Shannon ionic radii (CN = 8) for the five Ln/alkaline-earth cations relevant to this framework [4].

4.4 Hydration Behavior (TGA) — Nd End-Member

Segment (°C)	Mass change	Residual mass
802.7 → 800.0	−0.13%	98.52%
699.0 → 700.0	+0.02%	98.71%
598.7 → 600.0	+0.02%	98.90%
497.8 → 500.0	+0.03%	99.08%
397.1 → 400.0	+0.03%	99.21%
295.7 → 300.0	+0.07%	99.28%



Figure 9. TG mass vs. time under humid Ar (30–800 °C, 26.7 mg NBSCF). Mass falls on heating and rises on each cooling hold — the reversible pattern expected for hydration/dehydration at oxygen vacancies.

4.5 HRTEM and FFT — Nd End-Member

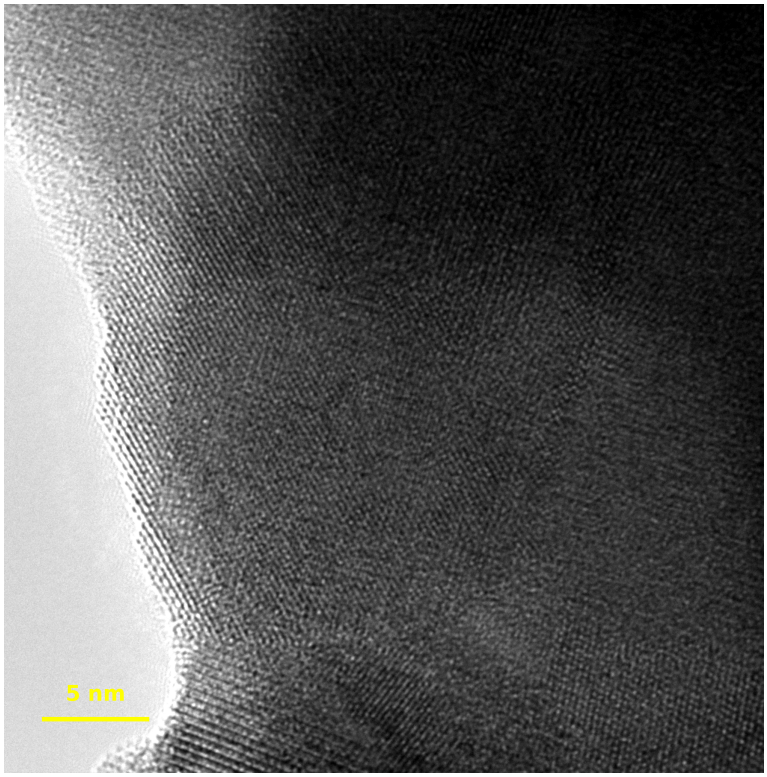


Figure 10a. HRTEM of an NBSCF particle edge showing crossed lattice fringes (image "0002", 5 nm scale bar).

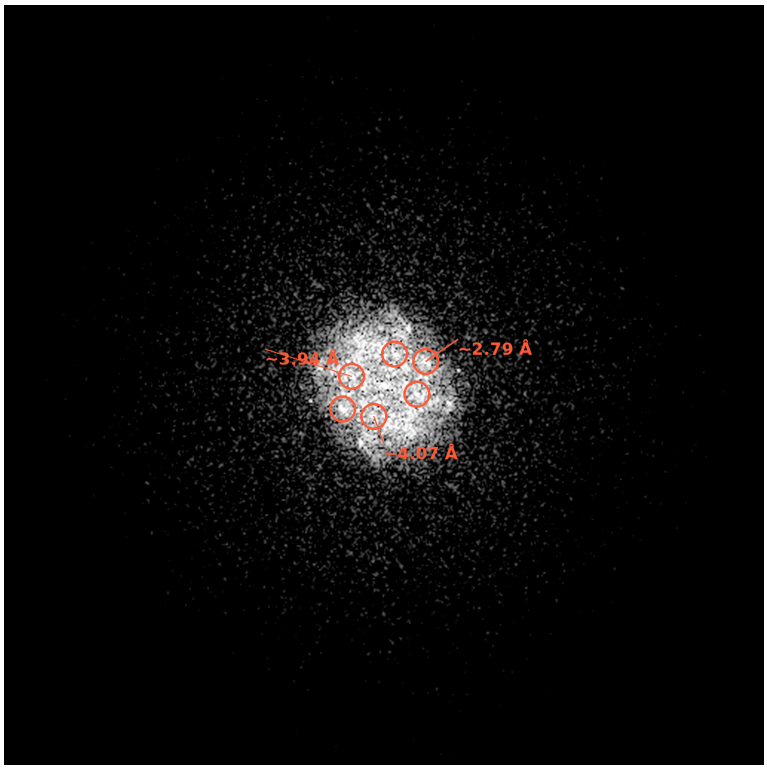


Figure 10b. FFT of the boxed lattice-fringe region. Measured spacings of ~3.94 Å, ~4.07 Å (two non-collinear {100}-type spots, ~87° apart) and ~2.79 Å (their vector-sum, {110}-type) are consistent with the refined cubic cell (d100 = 3.849 Å, d110 = 2.722 Å) within ~5%.

4.6 DC Conductivity

Sample	R (Ω)	H (cm)	A (cm²)	σ, R.T. (S cm⁻¹)
LaBSCF	1.1	0.1	0.14	0.649
NBSCF	1.2	0.12	0.31	0.323
Nd0.5Tb0.5BSCF	15	0.12	0.085	0.094
TbBSCF	29	0.1	0.39592	0.0087

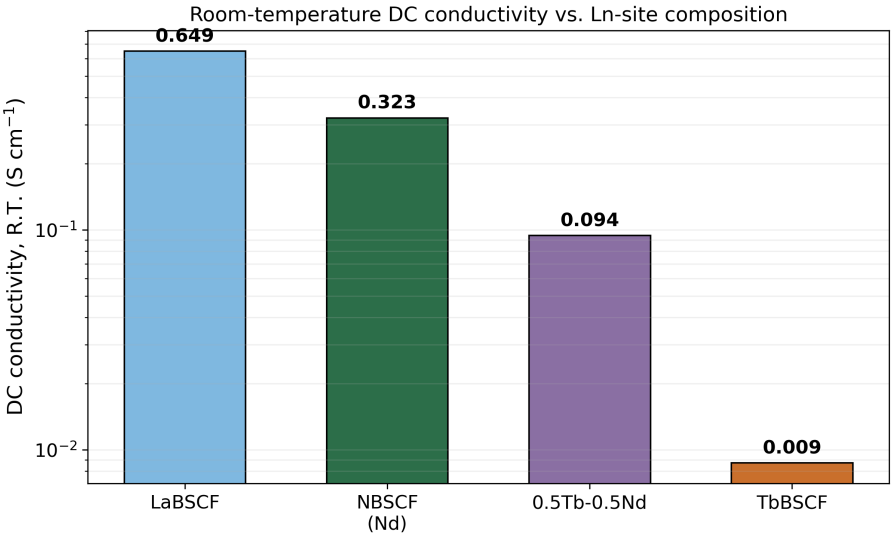


Figure 11. Room-temperature DC conductivity (log scale) vs. composition.

5. Discussion

Ionic-size-driven lattice response. The lattice parameter trend in Figure 7 is the clearest quantitative result of this project to date: substituting the larger La3+ (1.160 Å, CN = 8) for Nd3+ (1.109 Å) systematically expands the pseudo-cubic cell, while substituting the smaller Tb3+ (1.040 Å) contracts it — a textbook Vegard-type response to A-site ionic radius. The synchrotron-refined Nd end-member value (3.849 Å) falls essentially on the extrapolated trend line from the independently measured lab-XRD series, which is an internal consistency check between the two data sets and two different diffractometers/wavelengths.

Possible symmetry lowering at high Tb content. The resolved peak splitting seen only in the 75% and 100% Tb lab-XRD patterns (Fig. 6), together with the existence of a real, differently-symmetric tetragonal P4/mmm structural model for this framework (Section 4.2), together suggest that Tb-rich compositions may depart from cubic symmetry. This is consistent with (though not proven by) the smaller Tb3+ ionic radius increasing the tolerance-factor mismatch with the Ba/Sr/Co/Fe framework. This is presented as a hypothesis motivated by two independent observations, not a confirmed result — no Rietveld refinement has yet been performed on any Tb-rich composition.

Average vs. local structure. For the Nd end-member, the local (PDF) and average (Rietveld) lattice parameters agree within ~0.05%, and the XRD-only and joint XRD+PDF refinements agree on the cell edge despite differing O-content and fit statistics. Taken together, these do not show evidence of strong local distortion or clustering beyond what the average cubic model already captures, at the current data resolution.

Oxygen content and hydration. The refined oxygen content (2.57–2.85 out of 3 per formula unit, depending on refinement) confirms an oxygen-deficient perovskite, consistent with the reversible mass changes observed by TGA. The stepwise mass gain on each cooling hold (Section 4.4) is the expected signature of water uptake at oxygen vacancies, which is the mechanism that enables proton incorporation and transport relevant to PCEC/PCFC operation.

Conductivity trend. Room-temperature DC conductivity falls by roughly two orders of magnitude from LaBSCF to TbBSCF, in the same direction as decreasing Ln3+ ionic size. Because only four compositions have been measured, and by a simple two-terminal method that does not deconvolve contact resistance, this should be read as a qualitative trend rather than an intrinsic bulk conductivity value; the two lowest-conductivity samples are also the ones showing possible tetragonal distortion, so ionic size and symmetry change are confounded in this data set and cannot yet be separated.

TEM consistency. The HRTEM/FFT-derived spacings for the Nd end-member agree with the bulk-refined cubic cell within the precision expected of pixel-level FFT analysis, supporting that the nanoscale region imaged is representative of the bulk average structure measured by XRD/PDF.

6. Limitations and Future Work

- Full structural refinement (Rietveld/PDF) has only been performed on 1 of 16 compositions (the Nd end-member). The lab-XRD lattice parameters for the other 8 measured compositions are single-peak pseudo-cubic estimates, not refinements, and are explicitly approximate for the two Tb-rich compositions where the reflection is split.
- The two PrxTb1-x and PrxLa1-x families (8 of the 16 nominal compositions) have no characterization data yet beyond synthesis.
- TGA and HRTEM data exist only for the Nd end-member; it is not yet known whether the hydration behavior or nanoscale structure trends hold across the rest of the composition space.
- DC conductivity has been measured for 4 compositions at room temperature only, by a simple two-terminal method; contact resistance is not deconvolved and no high-temperature or humidity-dependent (proton-relevant) conductivity data exists yet.
- The tetragonal P4/mmm structural model is a preliminary (“rough”) refinement and should not be treated as final.
- Future work: complete lab XRD for the remaining Pr-containing compositions; Rietveld-refine the full Nd–La and Nd–Tb series to replace the pseudo-cubic estimates and confirm/refute the tetragonal transition; extend TGA, HRTEM, and conductivity measurements across the series; add high-temperature and wet/dry conductivity measurements; and move toward button-cell PCEC testing of the best-performing composition(s).

7. Conclusion

This project has established the target 16-composition Ln-substituted NBSCF library via a reproducible EDTA–citrate synthesis route, with transparent documentation of practical batch-size adjustments. Synchrotron XRD and PDF analysis of the Nd end-member confirm a cubic, oxygen-deficient triple-conducting perovskite, with XRD-only and joint XRD+PDF refinements reported separately to avoid conflating distinct results. Laboratory XRD across eight further compositions reveals a clear, ionic-radius-tracking lattice-parameter trend and flags a plausible cubic-to-tetragonal symmetry change at high Tb content that

warrants full refinement. TGA confirms reversible hydration behavior relevant to proton incorporation, HRTEM and FFT analysis of the Nd end-member are consistent with the refined bulk structure, and room-temperature DC conductivity across four compositions tracks the same ionic-size trend seen structurally. Together these results support the project's central hypothesis — that Ln-site ionic size systematically tunes structure and, plausibly, transport-relevant properties in this triple-conducting framework — while identifying exactly which compositions and measurements are needed to complete the picture.

References

[1] Ding, H.; Wu, W.; Jiang, C.; Ding, Y.; Bian, W.; Hu, B.; Singh, P.; Orme, C. J.; Wang, L.; Zhang, Y.; Ding, D. Self-sustainable protonic ceramic electrochemical cells using a triple conducting electrode for hydrogen and power production. Nat. Commun. 2020, 11, 1907.

[2] Papac, M.; Stevanović, V.; Zakutayev, A.; O'Hayre, R. Triple ionic-electronic conducting oxides for next-generation electrochemical devices. Nat. Mater. 2021, 20, 301–313.

[3] Feldhoff, A.; Arnold, M.; Martynczuk, J.; Gesing, T. M.; Wang, H. The stability of BSCF perovskite membranes under different oxygen partial pressures analyzed by high-temperature XRD. Solid State Sci. 2008, 10, 689–701.

[4] Shannon, R. D. Revised effective ionic radii and systematic studies of interatomic distances in halides and chalcogenides. Acta Cryst. 1976, A32, 751–767.